Geosci. Model Dev. Discuss., https://doi.org/10.5194/gmd-2018-340
Manuscript under review for journal Geosci. Model Dev.
Discussion started: 12 February 2019

Geoscientific Model Development Discussions
Open Access

Modeling extreme precipitation over East China with a global variable-resolution modeling framework (MPASv5.2): Impacts of resolution and physics

[1]Chun Zhao, [1]Mingyue Xu, [1]Yu Wang*, [1]Meixin Zhang, [2]Jianping Guo, [3]Zhiyuan Hu, [4]L. Ruby Leung, [5]Michael Duda, [5]William Skamarock

[1]School of Earth and Space Sciences, University of Science and Technology of China, Hefei, China
[2]State Key Laboratory of Severe Weather, Chinese Academy of Meteorological Sciences, Beijing, China
[3]Key Laboratory for Semi-Arid Climate Change of the Ministry of Education, Lanzhou University, Gansu, China
[4]Atmospheric Sciences and Global Change Division, Pacific Northwest National Laboratory, Richland, WA, USA
[5]National Center for Atmospheric Research, Boulder, CO, USA

*Corresponding authors: Yu Wang (wangyu09@ustc.edu.cn)

Key points:

1. MPAS simulations at global uniform and variable resolutions share similar characteristics of precipitation and wind in the refined region.
2. The experiments reveal the significant impacts of resolution on simulating the distribution and intensity of precipitation and updrafts.
3. Study provides the evidence supporting using convection-permitting global variable-resolution simulation for studying extreme precipitation.

Geosci. Model Dev. Discuss., https://doi.org/10.5194/gmd-2018-340
Manuscript under review for journal Geosci. Model Dev.
Discussion started: 12 February 2019

Abstract

The non-hydrostatic atmospheric Model for Prediction Across Scales (MPAS-A), a global variable-resolution modeling framework, is applied at a range of resolutions from hydrostatic (60 km, 30 km, 16 km) to non-hydrostatic (4 km) scales using regional refinement over East Asia to simulate an extreme precipitation event during 25-27 June 2012 over East China. The simulations are evaluated using ground observations and reanalysis data. The simulated distribution and intensity of precipitation are analyzed to investigate the sensitivity to model configuration, resolution, and physics parameterizations. In general, simulations using global uniform-resolution and variable-resolution meshes share similar characteristics of precipitation and wind in the refined region with comparable horizontal resolution. Further experiments at multiple resolutions reveal the significant impacts of horizontal resolution on simulating the distribution and intensity of precipitation and updrafts. More specifically, simulations at coarser resolutions shift the zonal distribution of the rainbelt and produce weaker heavy-precipitation centers that are misplaced relative to the observed locations. In comparison, simulations employing 4 km cell spacing produce more realistic features of precipitation and wind. Sensitivity experiments show that cloud microphysics have significant effects on modeling precipitation at non-hydrostatic scales, but their impacts are negligible compared to that of convective parameterizations for simulations at hydrostatic scales. This study provides the first evidence supporting the use of convection-permitting global variable-resolution simulations for studying and improving forecasting of extreme precipitation over East China, and motivates the need for a more systematic study of heavy precipitation events and impacts of physics parameterizations and topography in the future.

Geosci. Model Dev. Discuss., https://doi.org/10.5194/gmd-2018-340
Manuscript under review for journal Geosci. Model Dev.
Discussion started: 12 February 2019

Geoscientific Model Development Discussions
Open Access

1. Introduction

Extreme precipitation receives great attention because of its potential for generating flood, landslide, and other hazardous conditions. East China, occupied by more than 70% of the total population of China, is one of the areas with the most frequent intense extreme precipitation around the world (Zhai et al., 2005; Li et al., 2016). The socioeconomic development in regions such as the Yangtze River Delta region (YRD) in East China is remarkably vulnerable to extreme precipitation, making accurate forecast of extreme precipitation of great importance. The spatiotemporal variations of extreme precipitation over East China and their possible causes and underlying mechanisms have been investigated in many previous studies using observations and models (e.g., Ding et al., 2008; Zhang H. et al., 2011; Li et al., 2013; Zhang Q. et al., 2015, 2017; Hui et al., 2015; Liu et al., 2015; Li et al., 2016; Lin and Wang, 2016; Zhao et al., 2016; Zheng et al., 2016). Zhang et al. (2017) established a relationship between the western North Pacific subtropical high (WNPSH) and precipitation over East China and explored the underlying processes. Liu et al. (2015) analyzed data from the meteorological stations in East China and found significant increases in heavy precipitation at both rural and urban stations during 1955-2011. This enhanced precipitation intensity in East China has been partly attributed to localized daytime precipitation events (Guo et al., 2017). Recently, a regional climate model was used to simulate the regional climate extremes of China and noted large sensitivity of the simulated summer heavy precipitation over East China to the choice of cumulus parameterizations (Hui et al., 2015).

Numerical modeling is an important tool for understanding the underlying mechanisms of extreme precipitation and predicting precipitation characteristics that contributes to environmental impacts. Although precipitation modeling has improved in the last decades, accurate prediction of extreme precipitation remains challenging because of the multiscale nonlinear interactions of processes that generate heavy rainfall (Fritsch et al., 2004; Zhang et al., 2011; Sukovich et al. 2014). Previous studies suggested that increasing grid resolution could significantly improve modeling of extreme precipitation because the impacts of topography, land-use, land-atmosphere interaction, and other important processes are better resolved (e.g., Giorgi and Mearns, 1991; Giorgi and Marinucci, 1996; Leung et al., 2003; Bacmeister et al. 2014; ECMWF2016). With advances in computing and numerical modeling, convection-permitting modeling offers even more hope for reducing biases in simulating precipitation as convection and the strong vertical motions that are key to generating extreme precipitation are more explicitly resolved (Pedersen and Winther, 2005; Déqué et al., 2007;

Gao et al., 2017; Yang et al. 2017; Prein et al., 2015, 2017). Previous studies suggested that convection-permitting modeling is needed for more accurate prediction of the timing, distribution, and intensity of extreme precipitation events over China (e.g., Zhang et al., 2013; Xu et al., 2015).

Most studies of convection-permitting simulations have adopted non-hydrostatic regional models developed for weather forecasting or regional climate modeling (Prein et al. 2015). Global models capable of simulating non-hydrostatic dynamics are not as common as regional models, but they offer some advantages including the ability to provide global forecasts or simulations while avoiding numerical issues associated with lateral boundary conditions that are major sources of uncertainty in regional modeling and also limit regional feedback to global scale (e.g., Giorgi and Mearns, 1999; Wang et al. 2004; Laprise et al., 2008; Leung 2012; Prein et al. 2015). Non-hydrostatic global-variable resolution models, in particular, are useful as they allow convection-permitting simulations to be performed using regional refinement that significantly reduces computational cost compared to global convection-permitting modeling. So far, few studies used global variable-resolution models to investigate weather or climate simulations at convection-permitting scales (e.g., Prein et al., 2015). This study explores the use of a non-hydrostatic global variable resolution model, the Model for Prediction Across Scales (MPAS) for modeling an extreme precipitation event in East China.

MPAS is a new multiscale modeling approach developed to take advantage of advances in mesh generation by employing the spherical centroidal Voronoi tessellations (SCVTs) (Du et al. 1999; Ringler et al. 2008). The SCVTs in MPAS enable local mesh refinement through the mesh generation process where a specified scalar density function determines higher and lower resolution regions in the mesh (see, e.g., Ju et al. 2011). Meshes can be configured with multiple high-resolution regions, and high resolution in one region does not need to be balanced by coarser resolution elsewhere. The underlying theory of SCVTs is robust concerning mesh properties and mesh generation. The atmospheric solver in MPAS (Skamarock et al, 2012) integrates the non-hydrostatic equations, and as such it is suitable for both weather and climate simulation, i.e. for both nonhydrostatic and hydrostatic flow simulation. MPAS has been evaluated and used in previous studies for investigating the resolution impact on modeling clouds and precipitation (O'Brien et al., 2013; Zhao et al., 2016), the structure of the inter-tropical convergence zone (ITCZ) (Landu et al., 2014), precipitation extremes (Yang et al., 2014), atmospheric river frequency (Hagos et al., 2015), the position and strength of the eddy-driven jet (Lu et al., 2015), global atmospheric predictability at convection-permitting scales (Falko Judt, 2018), and regional climate modeling (Sakaguchi et al., 2015, 2016).

Geosci. Model Dev. Discuss., https://doi.org/10.5194/gmd-2018-340
Manuscript under review for journal Geosci. Model Dev.
Discussion started: 12 February 2019

To date, few studies have examined the MPAS performance in modeling extreme precipitation event, particularly at grid scales of ~10 km or less. In this study, we examine the MPAS performance in simulating a heavy precipitation event over East China and investigate its sensitivity to horizontal resolution and physics parameterizations. A heavy precipitation event that occurred on June 25-27 of 2012 over the YRD of East China is selected. During this period, a heavy precipitating system propagated along the Yangtze River and produced as much as 244 mm of precipitation in 24 hours at some locations. Simulations are performed using MPAS (v5.2) with different cumulus and microphysics schemes. We first compare simulations produced using a global mesh with uniform resolution and a global variable resolution mesh with a refined region that has the same resolution as that of the global uniform mesh. The goal is to demonstrate the fidelity of global variable resolution modeling relative to the more computationally expensive global high-resolution modeling approach in regions that share the same horizontal resolution. The impacts of resolutions at hydrostatic scales (with convective parameterizations) and non-hydrostatic scales (i.e., convection-permitting scales with convection processes largely resolved) are also examined. The MPAS simulations are evaluated against weather station observations from the National Meteorological Information Center of the China Meteorological Administration (CMA). In addition, the modeling results are also compared with the forecasts produced by the Global Forecast System (GFS) of the National Centers for Environmental Prediction (NCEP).

The rest of the paper is organized as follows. Section 2 describes briefly the MPAS model, the physics parameterizations, and the model configuration for this study, followed by a description of data for evaluation. The series of global uniform and variable resolution experiments are analyzed in section 3. The findings are then summarized in section 4.

2. Data and methodology

2.1 Model and experiments

2.1.1 MPAS-Atmosphere (MPAS-A) model

This study uses a fully compressible non-hydrostatic model (MPAS v5.2) developed for weather prediction and climate applications. The non-hydrostatic dynamical core of MPAS is described in Skamarock et al. (2012). MPAS uses C-grid staggering of the prognostic variables and centroidal Voronoi meshes to discretize the sphere. The unstructured spherical centroidal Voronoi tessellation (SCVT) generation algorithms can provide global quasi-uniform resolution meshes as well as variable-resolution meshes through the use of a single

Geosci. Model Dev. Discuss., https://doi.org/10.5194/gmd-2018-340
Manuscript under review for journal Geosci. Model Dev.
Discussion started: 12 February 2019

scalar density function, hence opening opportunities for regional downscaling and upscaling between mesoscales and non-hydrostatic scales to hydrostatic scales within a global framework. The vertical discretization uses the height-based hybrid terrain-following coordinate (Klemp, 2011), in which coordinate surfaces are progressively smoothed with height to remove the impact of small-scale terrain structures. The dynamical solver applies the split-explicit technique (Klemp et al., 2007) to integrate the flux-form compressible equations. The basic temporal discretization uses the third order Runge-Kutta scheme and explicit time-splitting technique (Wicker and Skamarock, 2002), similar to that used in the Weather Research and Forecasting (WRF) model (Skamarock et al., 2008). The scalar transport scheme used by MPAS on its Voronoi mesh is described in Skamarock and Gassmann (2011), and the monotonic option is used for all moist species. The extensive tests of MPAS using idealized and realistic cases verify that smooth transitions between the fine- and coarse-resolution regions of the mesh lead to no significant distortions of the atmospheric flow (e.g., Skamarock et al., 2012; Park et al., 2013).

In the current version (v5.2) of MPAS, there are a few physics schemes available. Three convective parameterizations can be used. The Kain-Fritsch (KF, Kain, 2004) and the new Tiedtke (NTD, Bechtold et al., 2004, 2008, 2014) schemes represent both deep and shallow convection using a mass flux approach with a convective available potential energy (CAPE) removal time scale (Kain, 2004). The third one, the GF scheme (Grell and Freitas, 2014), is based on the Grell-Devenyi ensemble scheme (Grell and Devenyi, 2002) using the multi-closure, multi-parameter, ensemble method but with improvements to smooth the transition to cloud-resolving scales following Arakawa et al. (2011). This scale-awareness is critical for global variable resolution simulation across hydrostatic (e.g., tens of km) and non-hydrostatic scales (e.g., 4 km). Fowler et al. (2016) implemented the GF convective parameterization in MPAS and examined the impacts of horizontal resolution on the partitioning between convective-parameterized and grid-resolved precipitation using a variable-resolution mesh in which the horizontal resolution varies between hydrostatic scales (~50 km) in the coarsest region of the mesh to non-hydrostatic scales (~ 3 km) in the most refined region of the mesh. For cloud microphysics, the WSM6 (Hong and Lim, 2006) and Thompson (Thompson et al., 2008) schemes are selected. Two options are available for representing the planetary boundary layer processes, the Mellor-Yamada-Nakanishi-Niino (MYNN) scheme (Nakanishi and Niino, 2006 and 2009) and the YSU scheme (Hong et al., 2006; Hong 2010). The Noah scheme (Chen and Dudhia, 2001) and the RRTMG scheme (Mlawer et al., 1997; Iacono et al., 2000) were implemented, respectively, for the land surface and radiative transfer processes.

2.1.2 Numerical experiments

In this study, the height coordinate of MPAS is configured with 55 layers, and the model top is at 30 km. Multiple experiments are conducted with MPAS using quasi-uniform resolution meshes and variable resolution meshes. Two quasi-uniform resolution meshes and three variable resolution meshes are configured, similar to those shown in Figure 1a and b that are coarsened to display the structure of the individual mesh cells. The quasi-uniform mesh has essentially the same mesh spacing globally, while the variable resolution mesh has finer mesh spacing in the refined region with a transition zone between the fine and coarse resolution meshes. More details about the mesh generation can be found in Ringler et al. (2011). The two quasi-uniform meshes have grid spacing that approximately equals to 15 km (U15km) and 60 km (U60km). The three variable resolution meshes feature a circular refined high-resolution region centered over East China as shown in Figure 1c. Figure 1c shows the exact mesh size distribution of the 4-60km variable resolution mesh (V4km) that has a refined region with grid spacing of approximately 4 km, and the mesh spacing gradually increases through a transition zone to approximately 60 km for the rest of the globe. The other two variable resolution meshes (V16km and V30km) have a similar mesh structure as the V4km mesh but with a mesh spacing of 16 km and 30 km, respectively, over the refined region that gradually increases to 128 km and 120 km, respectively, elsewhere.

Experiments U15km and V16km are compared to examine the difference between global uniform and variable resolution simulations in capturing the precipitation in the refined region, in order to explore the potential of regional refinement for regional weather and climate simulation. It is noteworthy here that the U15km mesh comprises ~2.5 million cells and the V16km mesh only comprises ~0.11 million cells. In order to investigate the potential impact from physics parameterizations, two available convective parameterizations (GF and NTD) are used for each experiment with the two meshes. Two cloud microphysics schemes (WSM6 and Thompson) are also tested, but the precipitation differences in the U15km and V16km experiments are small. Therefore, only the results using WSM6 with two different convective parameterizations are shown in this study for the two meshes (U15km.NTD, U15km.GF, V16km.NTD, and V16km.GF).

The U60km, V30km, V16km, and V4km experiments are conducted to quantify the impacts of horizontal resolution on simulating precipitation characteristics. As discussed above, GF is the only convective parameterization that has been tested with scale-aware capability and can be used across the hydrostatic (e.g., tens of km) and non-hydrostatic scales (e.g., 4 km).

Therefore, in order to investigate the difference among the experiments with the four meshes (U60km, V30km, V16km, and V4km), they are all conducted with the GF convective parameterization. Since the cloud microphysics has significant impact on the V4km simulations (discussed latter), the experiments of V4km with both WSM6 (V4km.WSM6) and Thompson (V4km.Thompson) cloud microphysics schemes are analyzed in this study. When examining the difference between the global uniform and variable resolution simulations and investigating the impact of mesh spacing, the same physics schemes and parameter values are used in multiple experiments if not specified explicitly. All the numerical experiments discussed above are summarized in Table 1.

To simulate the heavy precipitation event that occurred during June 25-27 of 2012 over the YRD of East China, all the MPAS experiments were initialized at 0000 UTC of 23 June 2012 to allow appropriate spin-up time, and the modeling results for 25-27 June 2012 are analyzed. The simulations were initialized using the forecast at 1° horizontal resolution at 0000 UTC of 23 June 2012 from the Global Forecast System (GFS) of National Center for Environmental Prediction (NCEP). This way, the MPAS simulation results can also be compared against the GFS forecast starting from the 0000 UTC of 23 June 2012.

2.2 Dataset

Several datasets are used to evaluate the MPAS simulations. The hourly precipitation dataset from CMA is used for evaluating the simulated precipitation characteristics. The distribution of stations over the study domain is shown as the color-filled circles in Figure 2. The 6-hourly wind field dataset from the ECMWF interim Reanalysis (ERA-interim) ($0.75^{o} \times 0.75^{o}$) (Dee et al., 2011) is used as the reference for evaluating the simulated distributions of winds. Lastly, the global forecast products at 0.5° and 1° horizontal resolutions starting from UTC00 of 23 June 2012 are also used for comparison. The GFS forecast products are downloaded from https://www.ncdc.noaa.gov/data-access/model-data/model-datasets/global-forcast-system-gfs. Since the focus of this study is not to investigate the difference between MPAS and GFS, details about the GFS are not discussed here but can be found on the website listed above.

3. Results

3.1 Simulations at quasi-uniform and variable resolutions

Figure 2 shows the spatial distributions of precipitation and wind at 850 hPa averaged during the event (June 25 00:00 to June 27 12:00 UTC Time) from the simulations with global uniform (15 km) and variable (16 km over East China) resolutions (U15km.NTD and V16km.NTD). The mean precipitation from the CMA stations and the winds from the ERA-interim reanalysis are also shown. The CMA observations show average precipitation rate exceeding 50 mm/day over central East China with a heavy rain belt extending from west to east. The rain belt is part of the Meiyu front that generates a large fraction of precipitation during the East Asian summer monsoon in China. In general, both simulations capture the observed precipitation pattern. It is evident that the modeling results over the refined region are consistent between the uniform and variable resolutions. The spatial correlation coefficient between the two simulations over the refined region (Fig. 2) is 0.85. Besides precipitation, both simulations also capture the distribution of winds from the reanalysis data. The wind fields between the two simulations are also consistent with a correlation coefficient of 0.99.

As mentioned above, the precipitation during this event is concentrated in a west-east narrow belt. For a more quantitative comparison, Figure 3 shows the zonal averaged precipitation during the event over East China (denoted as the black box in Fig. 2) from observations and simulations. The CMA observations show an evident precipitation peak reaching ~40 mm/day around the latitude of 31°N. All four simulations with different resolutions and convective parameterizations capture well the zonal distribution of observed precipitation. The correlation coefficients are 0.9 and 0.89 for the U15km and V16km simulations with the GF scheme, respectively, and 0.89 and 0.86 for the same simulations but with the NTD scheme. This comparison further indicates that the simulations at global uniform and variable resolutions are consistent with each other, with only negligible impacts from different convective parameterizations. Although this consistency does not depend on the convective schemes, simulations with the GF parameterization produce larger peak precipitation than those with the NTD parameterization and are more consistent with observations for this event. The impact of microphysics (WSM6 and Thompson) on modeling precipitation is also examined and is found to be negligible (not shown).

Figure 4 shows the meridional precipitation propagation over East China during the event. The CMA observations indicate that the rain belt propagates from 26°N at 06 UTC of 25 June to 31°N at 00 UTC of 26 June. The precipitation reaches the first peak around 00 UTC of 26 June. The rain belt stays around 31°N and reaches the second peak around 00 UTC of 27 June. The event ends around 12 UTC of 27 June. All four simulations generally reproduce the observed precipitation propagation. The correlation coefficients are 0.48 and 0.42 for the simulations with the GF scheme at the resolutions of U15km and V16km, respectively, and

0.55 and 0.54 for the simulations with the NTD scheme at the two resolutions. The results again indicate the consistency between the simulations at the global uniform and variable resolutions over the refined region. The convective and microphysics (not shown) parameterizations have negligible impact on modeling precipitation propagation during this event.

Overall, for the selected event, the MPAS simulations at global uniform and variable resolutions produce consistent results over the refined region with comparable horizontal resolution in terms of the spatial patterns of precipitation and wind fields and the precipitation propagation. This finding is in general agreement with the findings by previous studies of MPAS with idealized experiments (e.g., Zhao et al., 2016) and real-world experiments (e.g., Sakaguchi et al., 2015). These findings provide the basis for using global variable resolution configurations of MPAS for modeling extreme precipitation over East China. In the following, the impacts of resolution on modeling extreme precipitation during this event are investigated with multiple global variable-resolution experiments.

3.2 Impacts of resolution

3.2.1 Parameterized and resolved precipitation

Multiple experiments using MPAS at various resolutions are conducted as stated in the methodology section. The resolution crosses the scales from 60 km, 30 km, 16 km to 4 km. For global variable resolution configurations, a scale-aware convective parameterization is needed, especially for the configuration that crosses the hydrostatic (convective parameterization is required) and non-hydrostatic scales (convection-permitting). Therefore, the experiments analyzed below are all conducted with the GF scheme that is developed for simulations down to ~ 4 km resolution (details can be found in Grell and Freitas, 2014). To demonstrate the scale-aware performance of the GF convective parameterization across various resolutions, Figure 5 shows the spatial distributions of convective parameterized and resolved precipitation averaged during the event. At the resolution of 60 km and 16 km, precipitation produced from the convective parameterization dominates the total precipitation amount. On the contrary, at the resolution of 4 km, the total precipitation amount from simulations with two different microphysics is dominated by the resolved precipitation. This demonstrates that the GF scheme is aware of the resolution change so the precipitation from the simulations at convection-permitting scale is mostly produced by the cloud microphysics in MPAS.

3.2.2 Spatial and temporal variation

Figure 6 shows the observed and simulated spatial distributions of precipitation and wind fields at 850 hPa averaged during the event. For comparison, the GFS forecast results at the resolutions of 1.0 degree and 0.5 degree are also included. The GFS forecast results from the two resolutions are similar, both showing a northward shifted rain belt compared to the CMA observation. Due to the northern shift of the rain belt, the spatial correlation coefficients between the GFS and the CMA observations are only 0.06 and 0.03 for the resolutions of 1.0 degree and 0.5 degree, respectively. In comparison, the spatial correlation coefficients between the CMA observations and the MPAS simulations at the resolutions of 60 km, 30 km, and 16 km are 0.49, 0.47, and 0.56, respectively. The correlation coefficients for the 4 km simulations with the WSM6 and Thompson microphysics schemes are 0.63 and 0.54, respectively. In general, the experiments at the convection-permitting scale (4 km) capture better the observed precipitation pattern than simulations with convective parameterization over the refined region, although the performance is affected by the microphysics scheme to some extent. It is noteworthy that, although the difference in precipitation over East China is significant among the GFS forecasts at 0.5° and 1.0° resolutions and MPAS at various resolutions, their global distributions of precipitation and wind averaged during the event period are similar with spatial correlation coefficients of 0.40-0.43 and 0.86-0.93, respectively, against the satellite retrieved precipitation and ECMWF reanalysis wind (not shown).

Figure 7 shows the observed and simulated zonal distributions of precipitation averaged during the event over East China. For comparison, the GFS forecasts at 1°and 0.5° resolutions are also included. The modeling results are sampled at the CMA stations. Consistent with the spatial distributions of precipitation shown in Fig. 6, the GFS forecasts at both 0.5° and 1.0° resolutions reproduce the precipitation peak of ~40 mm/day but shift the rain belt northward by about 4.0° latitude from 31°N to 35°N. The MPAS simulations at 16 km and 30 km with the GF scheme can well capture the peak precipitation around 31°N, although the simulation at 30 km produces a second lower peak of precipitation around 29°N. The simulation at 60 km produces much lower precipitation peak of ~25 mm/day and shifts the rain belt southward to around 30°N. For the two MPAS simulations at 4 km, the precipitation is mainly generated by cloud microphysics (Fig. 5) and therefore can be significantly affected by the cloud microphysics schemes. The MPAS simulations at 4 km with WSM6 and Thompson produce different zonal distributions of the rain belt. The simulation using WSM6 reproduces the peak of precipitation fairly well, while the simulation using Thompson produces higher precipitation with a peak at 50 mm/day and shifts the peak northward by about 1 degree. Overall, the

Geosci. Model Dev. Discuss., https://doi.org/10.5194/gmd-2018-340
Manuscript under review for journal Geosci. Model Dev.
Discussion started: 12 February 2019

correlation coefficients between the CMA observations and the GFS forecasts are -0.19 and -0.15 for 0.5° and 1.0°, respectively, and the correlation coefficients are 0.68, 0.71, 0.89, and 0.97 (0.72) for the MPAS simulations at 60 km, 30 km, 16 km, and 4 km with the WSM6 (Thompson) cloud microphysics.

Figure 8 compares the observed and simulated precipitation propagation during the event over East China. The modeling results are sampled at the CMA stations. The GFS forecasts at 0.5° and 1.0° are similar, both generate a heavy precipitation zone between 34°N and 35°N that lasts for about 18 hours from UTC12 of June 26. This is largely different from the CMA observations, so the correlation coefficients between the forecasts and observations are only 0.02 and 0.03 for 0.5° and 1.0°, respectively. The MPAS simulations are highly dependent on the resolutions. All simulations reproduce the two peaks of precipitation at roughly the same time as observed during the event. However, the experiment at 60 km simulates the first precipitation peak southward and the second peak northward of the observations, while the experiment at 30 km simulates the second peak further south. The correlation coefficients are 0.30 and 0.32 between the observations and the simulations at 60 km and 30 km, respectively. The experiments at 16 km and 4 km can well capture the timing and latitude of the observed precipitation event, except that the experiment at 4 km with the Thompson scheme overestimates the precipitation amount of the first peak. The correlation coefficients are 0.41 and 0.42 (0.38) for 16 km and 4 km with the WSM6 (Thompson) cloud microphysics schemes, respectively.

Figure 9 compares the height-latitude cross section of the winds averaged over the region (shown as in Fig. 6) during the event from the ERA-interim reanalysis, the GFS forecasts, and the MPAS simulations. In the ERA-interim reanalysis wind fields, vertical motion is located primarily around 31°N, extending from the lower troposphere (~900 hPa) to the upper troposphere (~200 hPa). The GFS simulates the vertical motion primarily around 33°N, but the vertical motion is also strong around 35°N from 600 hPa to 200 hPa, which can be linked to the heavy precipitation generated there. These biases result in weaker correlation in vertical winds between the reanalysis and the GFS forecasts with coefficients of 0.25 and 0.22 for 0.5° and 1.0° resolutions, respectively. The MPAS experiment at 60 km simulates the vertical motion toward the south around 28°N. The MPAS experiments at 30 km and 16 km generally agree well with the ERA-interim reanalysis, although both generate higher vertical motion in the south (e.g. 25°N) to some extent. The correlation coefficients between the reanalysis and the MPAS experiments at 60 km, 30 km, and 16 km are 0.57, 0.76, and 0.80, respectively. The

Geosci. Model Dev. Discuss., https://doi.org/10.5194/gmd-2018-340
Manuscript under review for journal Geosci. Model Dev.
Discussion started: 12 February 2019

Geoscientific Model Development Discussions Open Access

MPAS experiment at 4 km with the WSM6 scheme produces consistent vertical motion with that in the ERA-interim reanalysis, while the one with the Thompson scheme shifts the vertical motion a little further north. Both experiments at 4 km have the highest correlation in the distributions of vertical motion with the reanalysis with coefficients of 0.85 and 0.81 for WSM6 and Thompson, respectively. The zonal distributions of precipitation discussed above correspond well with the distributions of vertical motion in all the experiments. Differences in the spatial distribution of vertical motions suggest that model resolution, and in some degree cloud microphysics parameterizations, have important effects on simulating the structure of the Meiyu front and the embedded precipitation.

3.2.3 Distribution of extreme precipitation

Besides predicting the spatial and temporal variations of the rain belt, it is also critical to capture the location and intensity of extreme precipitation within the heavy rain belt. Since the GFS forecasts shift the entire rain belt northward, only the MPAS simulations are analyzed here. Figure 10 shows the spatial distributions of precipitation averaged during the event over the heavy rain region (27°N-32°N and 110°E-122°E). The CMA observations show that heavy precipitation exceeding 50 mm/day mainly occurs over the plains of South Anhui province and Southeast Hubei province and part of the Huang Mountains. The MPAS experiment at 60 km simulates much smaller areas with heavy precipitation exceeding 50 mm/day. In addition, it simulates heavy precipitation over some areas of Hunan province, which is not observed by the CMA stations. The experiment at 30 km produces more numerous areas with heavy precipitation and captures the locations of heavy precipitation over the Huang Mountains. However, it misses the heavy precipitation over the plains of South Anhui province and Southeast Hubei province; instead, it produces heavy precipitation over large areas of mountainous regions over Hunan and Jiangxi provinces. The experiment at 16 km simulates better spatial distribution of heavy precipitation, particularly capturing the heavy precipitation over the Huang Mountains and the plain of South Anhui province, although it still shifts the heavy precipitation from Southeast Hubei province to Hunan province. The experiments at 4 km are affected by the cloud microphysics. The 4 km experiment with the WSM6 scheme produces the best spatial distribution among the MPAS experiments. It generally reproduces the observed heavy precipitation areas during this event. On the other hand, the 4 km experiment with the Thompson microphysics produces more areas of heavy precipitation over Central Anhui province. As a result, the correlation coefficients between the observations and the MPAS experiments at the resolutions of 60 km, 30 km, 16 km, and 4 km are 0.20, 0.21, 0.29, 0.50 (WSM6), and 0.42 (Thompson), respectively.

Figure 11 shows the probability density functions (PDFs) of hourly precipitation at all the CMA stations during the event. Precipitation above ~5 mm/hour (~120 mm/day) is considered very heavy and extra heavy storm rain event (refer to the CMA definition) that may cause dramatic flooding and damage locally or regionally. During this event, for precipitation lower than ~5 mm/hour, the MPAS simulations at hydrostatic scales (60 km, 30 km, and 16 km) overestimate the frequency, while above ~5 mm/hour, these simulations significantly underestimate the frequency. In contrast, the MPAS simulations at convection-permitting scale (4 km) produce much higher frequency of extreme precipitation above ~5 mm/hour, more consistent with the observations. However, the simulated frequency of extreme precipitation at convection-permitting scale depends on the cloud microphysics schemes. The Thompson scheme produces much higher frequency than the WSM6 scheme and results in a positive bias relative to the observations during this event, which deserves further investigation in future. The results also indicate that the convective parameterization appears not to be able to produce the higher intensity precipitation.

Previous studies found that the distribution of extreme precipitation correlates well with that of the lower tropospheric upward vertical velocity (e.g., Zhao et al., 2016). Figure 12 shows the PDFs of hourly upward vertical velocity averaged below 700 hPa at all the CMA stations during the event from the MPAS simulations. In general, the comparison of lower-level upward vertical velocity among the experiments is consistent with that of precipitation (Fig. 11) in that simulations at hydrostatic scales (i.e., 60 km, 30 km, and 16 km in this study) produce higher frequencies of updrafts < 4 cm/s than simulations at 4 km and vice versa for stronger updrafts. The difference in updrafts between the 4 km MPAS simulations with two different cloud microphysics schemes is negligible. Another analysis with the simulated updrafts at various resolutions all regridded to 0.5° resolution shows the similar PDFs as Fig. 12.

4. Summary and discussion

In this study, a series of MPAS simulations of a heavy precipitation event over East China at various resolutions from hydrostatic (60 km, 30 km, 16 km) to non-hydrostatic (4 km) scales are analyzed. The consistency between the MPAS simulations at global uniform and variable resolutions is also investigated. Besides the impacts of resolution on simulating heavy precipitation, the impacts of convective and cloud microphysics schemes are also examined.

Geosci. Model Dev. Discuss., https://doi.org/10.5194/gmd-2018-340
Manuscript under review for journal Geosci. Model Dev.
Discussion started: 12 February 2019

All the MPAS simulations are evaluated using the CMA station observations of precipitation and the ERA-interim reanalysis of winds, and compared against the NCEP GFS forecasts that share the same initial condition of the MPAS simulations.

In general, the MPAS simulations at global uniform (U15km) and variable (V16km) resolutions produce similar results in terms of the spatial and temporal distributions of precipitation and winds inside the refined region over East China. Both the experiments can capture the observed precipitation characteristics. This suggests that the global variable-resolution configuration of MPAS may be appropriate to simulate heavy precipitation over East China, which is also consistent with the finding from previous studies using variable resolution MPAS with regional refinement over other parts of the globe (e.g., Sakaguchi et al., 2015; Zhao et al., 2016). The simulations with two different convective parameterizations show that the MPAS simulated distributions of precipitation are affected by the convective schemes at hydrostatic scales, while the impacts from the cloud microphysics schemes are small (not shown).

Further investigation of MPAS experiments at multiple resolutions from hydrostatic (60 km, 30 km, 16 km) to non-hydrostatic (4 km) scales over East China shows significant impacts of resolution on simulating the spatial distributions of precipitation and winds. The variable-resolution simulations spanning hydrostatic and non-hydrostatic scales reveal that the scale-aware GF convective parameterization produces less convective parameterized precipitation as the horizontal resolution increases. Meanwhile, the subgrid-scale motions become increasingly resolved and the ratio of grid-scale to total precipitation increases over the refined region as resolution increases to 4 km. Comparison against the station observations indicates that the MPAS simulations at 16 km and 4 km can generally well capture the observed temporal and zonal distribution of the rain belt in the simulated event. The simulations at coarser resolutions of 60 km and 30 km produce weaker precipitation and a southward shift of the rain belt. In contrast, the GFS forecasts at 0.5° and 1.0° produce a northward shift of the rain belt. The biases in the locations of rain belt are consistent with the zonal shift of vertical motion. This suggests that the position of the Meiyu front that produces the vertical motion is sensitive to the models and their specific configurations even though all simulations share the same initial condition. The analysis also indicates the significant impacts from cloud microphysics on the MPAS simulations at 4 km in terms of precipitation distribution and intensity.

Geosci. Model Dev. Discuss., https://doi.org/10.5194/gmd-2018-340
Manuscript under review for journal Geosci. Model Dev.
Discussion started: 12 February 2019

Besides the general zonal distribution of the rain belt, the distribution and intensity of heavy precipitation are also investigated. Among the MPAS experiments with multiple resolutions, only the simulations at 4 km can capture the observed locations of heavy precipitation. All experiments at coarser resolutions miss some areas of heavy precipitation or produce heavy precipitation in areas different from that observed. In addition, only the MPAS simulations at 4 km can generate reasonable frequency of intense precipitation that is significantly underestimated by simulations at coarser resolutions, which may indicate that the convective parameterization appears not to be able to produce intense precipitation. The analysis also shows that the underestimation of intense precipitation is consistent with the underestimation of resolved upward motions in the simulations at coarser resolutions.

Although the MPAS simulations at 4 km produce the best results among the experiments at various resolutions, they still have some biases in the timing and intensity of precipitation. In addition, the performance of MPAS at convection-permitting scale is quite sensitive to the cloud microphysics scheme in terms of the distribution and intensity of extreme precipitation. This is consistent with Feng et al. (2018), who found that cloud microphysics parameterizations in convection permitting regional simulations have important effects on macroscale properties such as the lifetime, precipitation amount, stratiform versus convective rain volumes of mesoscale convective systems in the U.S. They attributed the impacts to the representation of ice phase hydrometeor species that influence the mesoscale convective systems through their influence on the diabatic heating profiles that provide dynamical feedback to the circulation (Yang et al. 2017). Hence more efforts may be needed to improve cloud microphysics processes for modeling extreme precipitation at convection-permitting scale in the future. In the meantime, aerosols have been found to play a critical role in simulating some heavy precipitation events over China through their impacts on cloud microphysics and/or radiation (e.g., Zhong et al., 2015, 2017; Fan et al., 2015). The current version of MPAS does not represent aerosol-radiation and aerosol-cloud interactions, which may also contribute to the biases of extreme precipitation at convection-permitting scales. Lastly, it is also noteworthy that the resolution of 4 km may still be insufficient to resolve well some convective cells, which may also contribute to the modeling biases (Bryan and Morrison, 2012).

This study provides the first evidence supporting the use of global variable resolution configuration of MPAS for simulating extreme precipitation events over East China. In particular, the MPAS variable-resolution experiment at convection-permitting scale (4 km) improves the simulated distribution and intensity of precipitation over the area of interest,

Geosci. Model Dev. Discuss., https://doi.org/10.5194/gmd-2018-340
Manuscript under review for journal Geosci. Model Dev.
Discussion started: 12 February 2019

Geoscientific Model Development Discussions
Open Access EGU

which is consistent with previous studies using regional convection permitting models (e.g., Zhang et al., 2013; Prein et al., 2015; Yang et al. 2017; Gao et al. 2017; Feng et al. 2018). The higher resolution MPAS experiments simulate better spatial distribution of heavy precipitation over the complex topographic region of East China, which suggests that topography may play a critical role and deserves further investigation in the future. Although the GFS forecasts analyzed in this study show significant biases in precipitation distribution, some GFS forecasts initialized at different times are found to produce more reasonable results (not shown), supporting the need for ensemble modeling for forecasting extreme events. However, the zonal shift of the rain belt by the MPAS simulations at coarser resolutions compared to simulations at finer resolutions suggests that resolution may have contributed to the GFS forecast biases. A more detailed exploration of the differences between the MPAS and GFS simulations is beyond the scope of this study. Finally, some studies noted that convection-permitting modeling does not always add values in simulating heavy precipitation compared to hydrostatic scale modeling (e.g., Kain et al., 2008). Our results show that cloud microphysics parameterizations have important effects in convection permitting simulations, but modeling of other physical processes such as boundary layer turbulence, radiation, and aerosols may also affect the skill of convection permitting simulations. Furthermore, more events of heavy precipitation over East China should be investigated in the future to more systematically evaluate the MPAS variable-resolution modeling framework and the impacts of resolution and physical parameterizations.

Code availability

The MPAS release v5.2 can be obtained at *mpas-dev.github.io*. Global meshes generated for the experiments used in this study are available upon request by contacting the corresponding author.

Author contributions

CZ and YW designed research. MX performed the simulations. CZ, MX, MZ, and ZH analyzed the simulations. JG collected and analyzed the observations. CZ, MX, and YW wrote the paper. LRL, MD, and WS guided the experiment design and edited the paper.

Acknowledgements

This research was supported by the Ministry of Science and Technology of China under grant 2017YFC1501401, the Thousand Talents Plan for Young Professionals, the Fundamental Research Funds for the Central Universities, and the National Natural Science Foundation of China (grant 41775146). The study used computing resources from the High-Performance Computing Center of University of Science and Technology of China (USTC) and the TH-2 of National Supercomputer Center in Guangzhou (NSCC-GZ). Leung was supported by the U.S. Department of Energy Office of Science Biological and Environmental Research as part of the Regional and Global Modeling and Analysis program. PNNL is operated for the Department of Energy under contract DE-AC05-76RL01830.

Reference

Arakawa, A., Jung, J. H., & Wu, C. M.: Toward unification of the multiscale modeling of the atmosphere, Atmospheric Chemistry and Physics, 11(8), 3731-3742, https://doi.org/10.5194/acp-11-3731-2011, 2011.

Bacmeister, J. T., Wehner, M. F., Neale, R. B., Gettelman, A., Hannay, C., Lauritzen, P. H., ... & Truesdale, J. E.: Exploratory high-resolution climate simulations using the Community Atmosphere Model (CAM), Journal of Climate, 27(9), 3073-3099, https://doi.org/10.1175/JCLI-D-13-00387.1, 2014.

Bechtold, P., Chaboureau, J. P., Beljaars, A., Betts, A. K., Köhler, M., Miller, M., & Redelsperger, J. L.: The simulation of the diurnal cycle of convective precipitation over land in a global model, Quarterly Journal of the Royal Meteorological Society, 130(604), 3119-3137, https://doi.org/10.1256/qj.03.103, 2004.

Bechtold, P., Köhler, M., Jung, T., Doblas-Reyes, F., Leutbecher, M., Rodwell, M. J., ... & Balsamo, G.: Advances in simulating atmospheric variability with the ECMWF model: From synoptic to decadal time-scales, Quarterly Journal of the Royal Meteorological Society, 134(634), 1337-1351, https://doi.org/10.1002/qj.289, 2008.

Bechtold, P., Semane, N., Lopez, P., Chaboureau, J. P., Beljaars, A., & Bormann, N.: Representing equilibrium and nonequilibrium convection in large-scale models, Journal of the Atmospheric Sciences, 71(2), 734-753, https://doi.org/10.1175/JAS-D-13-0163.1, 2014.

Bryan, G. H., and H. Morrison: Sensitivity of a simulated squall line to horizontal resolution and parameterization of microphysics, Mon. Wea. Rev., 140, 202–225, https://doi.org/10.1175/MWR-D-11-00046.1, 2012.

Chauvin, F., J.-F. Royer, and M. Deque: Response of hurricane type vortices to global warming as simulated by ARPEGE-Climat at high resolution, Climate Dyn., 27, 377-399, https://doi.org/10.1007/s00382-006-0135-7, 2006.

Chen, F., & Dudhia, J.: Coupling an advanced land surface–hydrology model with the Penn State–NCAR MM5 modeling system. Part I: Model implementation and sensitivity, Monthly Weather Review, 129(4), 569-585, https://doi.org/10.1175/1520-0493(2001)129<0569:CAALSH>2.0.CO;2, 2001.

Dee, D. P., Uppala, S. M., Simmons, A. J., Berrisford, P., Poli, P., Kobayashi, S., ... & Bechtold, P.: The ERA- Interim reanalysis: Configuration and performance of the data assimilation system, Quarterly Journal of the royal meteorological society, 137(656), https://doi.org/10.1002/qj.828, 2011.

Déqué, M., Jones, R. G., Wild, M., Giorgi, F., Christensen, J. H., Hassell, D. C., ... & De Castro, M.: Global high resolution versus Limited Area Model climate change projections over Europe: quantifying confidence level from PRUDENCE results, Climate Dynamics, 25(6), 653-670, https://doi.org/10.1007/s00382-005-0052-1, 2005.

Déqué, M., & Piedelievre, J. P.: High resolution climate simulation over Europe, Climate dynamics, 11(6), 321-339, https://doi.org/10.1007/BF00215735, 1995.

Déqué, M., Rowell, D. P., Lüthi, D., Giorgi, F., Christensen, J. H., Rockel, B., ... & van den Hurk, B. J. J. M.: An intercomparison of regional climate simulations for Europe: assessing uncertainties in model projections, Climatic Change, 81(1), 53-70, https://doi.org/10.1007/s10584-006-9228-x, 2007.

Ding, Y., Wang, Z., & Sun, Y.: Inter-decadal variation of the summer precipitation in East China and its association with decreasing Asian summer monsoon. Part I: Observed evidences. International Journal of Climatology, 28(9), 1139-1161, https://doi.org/10.1002/joc.1615, 2008.

Du, Q., Faber, V., & Gunzburger, M.: Centroidal Voronoi tessellations: Applications and algorithms. SIAM review, 41(4), 637-676, https://doi.org/10.1137/S0036144599352836, 1999.

ECMWF: ECMWF strategy 2016–2025: The strength of a common goal. European Centre for Medium-Range Weather Forecasts Tech. Rep., 32 pp, https://www.ecmwf.int/sites/default/files/ECMWF_Strategy_2016-2025.pdf, 2016.

Fan, J., Rosenfeld, D., Yang, Y., Zhao, C., Leung, L. R., & Li, Z.: Substantial contribution of anthropogenic air pollution to catastrophic floods in Southwest China, Geophysical Research Letters, 42(14), 6066-6075, https://doi.org/10.1002/2015GL064479, 2015.

Feng, Z., L.R. Leung, R.A. Houze, Jr., S. Hagos, J. Hardin, Q. Yang. B. Han, & J. Fan: Structure and evolution of mesoscale convective systems: sensitivity to cloud microphysics in convection-permitting simulations over the US, J. Adv. Model. Earth Syst., 10, doi: 10.1029/2018MS001305, 2018.

Fowler, L. D., Skamarock, W. C., Grell, G. A., Freitas, S. R., & Duda, M. G.: Analyzing the Grell–Freitas convection scheme from hydrostatic to nonhydrostatic scales within a global model, Monthly Weather Review, 144(6), 2285-2306, https://doi.org/10.1175/MWR-D-15-0311.1, 2016.

Geosci. Model Dev. Discuss., https://doi.org/10.5194/gmd-2018-340
Manuscript under review for journal Geosci. Model Dev.
Discussion started: 12 February 2019

Geoscientific Model Development
Discussions
Open Access

Fox-Rabinovitz, M., Côté, J., Dugas, B., Déqué, M., & McGregor, J. L.: Variable resolution general circulation models: Stretchedlgrid model intercomparison project (SGMIP), Journal of Geophysical Research: Atmospheres, 111(D16), https://doi.org/10.1029/2005JD006520, 2006.

Fox-Rabinovitz, M. S., Stenchikov, G. L., Suarez, M. J., & Takacs, L. L.: A finite-difference GCM dynamical core with a variable-resolution stretched grid, Monthly Weather Review, 125(11), 2943-2968, https://doi.org/10.1175/1520-0493(1997)125<2943:AFDGDC>2.0.CO;2, 1997.

Fritsch, J. M., & Carbone, R. E.: Improving quantitative precipitation forecasts in the warm season: A USWRP research and development strategy, Bulletin of the American Meteorological Society, 85(7), 955-966, https://doi.org/10.1175/BAMS-85-7-955, 2004.

Gao, Y., L.R. Leung, C. Zhao, & S. Hagos: Sensitivity of summer precipitation to model resolution and convective parameterizations across gray zone resolutions, J. Geophys. Res., 122, 2714-2733, https://doi.org/10.1002/2016JD025896, 2017.

Giorgi, F., & Marinucci, M. R.: A investigation of the sensitivity of simulated precipitation to model resolution and its implications for climate studies, Monthly Weather Review, 124(1), 148-166, https://doi.org/10.1175/1520-0493(1996)124<0148:AIOTSO>2.0.CO;2, 1996.

Giorgi, F., & Mearns, L. O.: Approaches to the simulation of regional climate change: a review, Reviews of Geophysics, 29(2), 191-216, https://doi.org/10.1029/90RG02636, 1991.

Grell, G. A., & Dévényi, D.: A generalized approach to parameterizing convection combining ensemble and data assimilation techniques, Geophysical Research Letters, 29(14), 38-1, https://doi.org/10.1029/2002GL015311, 2002.

Grell, G. A., & Freitas, S. R.: A scale and aerosol aware stochastic convective parameterization for weather and air quality modeling, Atmos. Chem. Phys, 14(10), 5233-5250, https://doi.org/10.5194/acp-14-5233-2014, 2014.

Guo, J., Su, T., Li, Z., Miao, Y., Li, J., Liu, H., Xu, H., Cribb, M. & Zhai, P.: Declining frequency of summertime local-scale precipitation over eastern China from 1970 to 2010 and its potential link to aerosols, Geophysical Research Letters, 44(11), 5700-5708, https://doi.org/10.1002/2017GL073533, 2017.

Hagos, S., Leung, L. R., Yang, Q., Zhao, C., & Lu, J.: Resolution and dynamical core dependence of atmospheric river frequency in global model simulations, Journal of Climate, 28(7), 2764-2776, https://doi.org/10.1175/JCLI-D-14-00567.1, 2015.

Hong, S. Y.: A new stable boundary‐layer mixing scheme and its impact on the simulated East Asian summer monsoon, Quarterly Journal of the Royal Meteorological Society, 136(651), 1481-1496, https://doi.org/10.1002/qj.665, 2010.

Hong, S. Y., & Lim, J. O. J.: The WRF single-moment 6-class microphysics scheme (WSM6), J. Korean Meteor. Soc, 42(2), 129-151, 2006.

Hong, S. Y., Noh, Y., & Dudhia, J.: A new vertical diffusion package with an explicit treatment of entrainment processes, Monthly weather review, 134(9), 2318-2341, https://doi.org/10.1175/MWR3199.1, 2006.

Hui, P., Tang, J., Wang, S., & Wu, J.: Sensitivity of simulated extreme precipitation and temperature to convective parameterization using RegCM3 in China, Theoretical and applied climatology, 122(1-2), 315-335, https://doi.org/10.1007/s00704-014-1300-2, 2015.

Iacono, M. J., Mlawer, E. J., Clough, S. A., & Morcrette, J. J.: Impact of an improved longwave radiation model, RRTM, on the energy budget and thermodynamic properties of the NCAR community climate model, CCM3, Journal of Geophysical Research: Atmospheres, 105(D11), 14873-14890, https://doi.org/10.1029/2000JD900091,2000.

Judt, F.: Insights into Atmospheric Predictability through Global Convection-Permitting Model Simulations, Journal of the Atmospheric Sciences, 75(5), 1477-1497, https://doi.org/10.1175/JAS-D-17-0343.1, 2018.

Ju, L., Ringler, T., & Gunzburger, M.: Voronoi tessellations and their application to climate and global modeling, In Numerical techniques for global atmospheric models (pp. 313-342), Springer, Berlin, Heidelberg. https://doi.org/10.1007/978-3-642-11640-7_10, 2011.

Kain, J. S.: The Kain–Fritsch convective parameterization: an update, Journal of applied meteorology, 43(1), 170-181, https://doi.org/10.1175/1520-0450(2004)043<0170:TKCPAU>2.0.CO;2, 2004.

Kain, J. S., Weiss, S. J., Bright, D. R., Baldwin, M. E., Levit, J. J., Carbin, G. W., ... & Thomas, K. W.: Some practical considerations regarding horizontal resolution in the first generation of operational convection-allowing NWP, Weather and Forecasting, 23(5), 931-952, https://doi.org/10.1175/WAF2007106.1, 2008.

Geosci. Model Dev. Discuss., https://doi.org/10.5194/gmd-2018-340
Manuscript under review for journal Geosci. Model Dev.
Discussion started: 12 February 2019

Geoscientific Model Development Discussions
Open Access
EGU

Klemp, J. B.: A terrain-following coordinate with smoothed coordinate surfaces, Monthly weather review, 139(7), 2163-2169, https://doi.org/10.1175/MWR-D-10-05046.1, 2011.

Klemp, J. B., Skamarock, W. C., & Dudhia, J.: Conservative split-explicit time integration methods for the compressible nonhydrostatic equations, Monthly Weather Review, 135(8), 2897-2913, https://doi.org/10.1175/MWR3440.1, 2007.

Landu, K., Leung, L. R., Hagos, S., Vinoj, V., Rauscher, S. A., Ringler, T., & Taylor, M.: The dependence of ITCZ structure on model resolution and dynamical core in aquaplanet simulations, Journal of Climate, 27(6), 2375-2385, https://doi.org/10.1175/JCLI-D-13-00269.1, 2014.

Laprise, R.: Regional climate modelling, Journal of Computational Physics, 227(7), 3641-3666, https://doi.org/10.1016/j.jcp.2006.10.024, 2008.

Leung, L. R., & Qian, Y.: The sensitivity of precipitation and snowpack simulations to model resolution via nesting in regions of complex terrain, Journal of Hydrometeorology, 4(6), 1025-1043, https://doi.org/10.1175/1525-7541(2003)004<1025:TSOPAS>2.0.CO;2, 2003.

Li, J., Zhang, Q., Chen, Y. D., & Singh, V. P.: GCMs-based spatiotemporal evolution of climate extremes during the 21st century in China, Journal of Geophysical Research: Atmospheres, 118(19), https://doi.org/10.1002/jgrd.50851, 2013.

Li, W., Jiang, Z., Xu, J., & Li, L.: Extreme Precipitation Indices over China in CMIP5 Models. Part II: Probabilistic Projection, Journal of Climate, 29(24), 8989-9004, https://doi.org/10.1175/JCLI-D-16-0377.1, 2016.

Li, Z., W. K.-M. Lau, V. Ramanathan et al.: Aerosol and monsoon climate interactions over Asia, *Rev. Geophys.*, 54, https://doi.org/10.1002/2015RG000500, 2016.

Lin, Z., & Wang, B.: Northern East Asian low and its impact on the interannual variation of East Asian summer rainfall, Climate dynamics, 46(1-2), 83-97, https://doi.org/10.1007/s00382-015-2570-9, 2016.

Liu, R., Liu, S. C., Cicerone, R. J., Shiu, C. J., Li, J., Wang, J., & Zhang, Y.: Trends of extreme precipitation in eastern China and their possible causes, Advances in Atmospheric Sciences, 32(8), 1027-1037, https://doi.org/10.1007/s00376-015-5002-1, 2015.

Lorant, V., & Royer, J. F.: Sensitivity of equatorial convection to horizontal resolution in aquaplanet simulations with a variable-resolution GCM, Monthly weather

Geosci. Model Dev. Discuss., https://doi.org/10.5194/gmd-2018-340
Manuscript under review for journal Geosci. Model Dev.
Discussion started: 12 February 2019

review, 129(11), 2730-2745, https://doi.org/10.1175/1520-0493(2001)129<2730:SOECTH>2.0.CO;2, 2001.

Lu, J., Chen, G., Leung, L. R., Burrows, D. A., Yang, Q., Sakaguchi, K., & Hagos, S.: Toward the dynamical convergence on the jet stream in aquaplanet AGCMs, Journal of Climate, 28(17), 6763-6782, https://doi.org/10.1175/JCLI-D-14-00761.1, 2015.

Medvigy, D., Walko, R. L., Otte, M. J., & Avissar, R.: Simulated changes in northwest US climate in response to Amazon deforestation, Journal of Climate, 26(22), 9115-9136, https://doi.org/10.1175/JCLI-D-12-00775.1, 2013.

Mlawer, E. J., Taubman, S. J., Brown, P. D., Iacono, M. J., & Clough, S. A.: Radiative transfer for inhomogeneous atmospheres: RRTM, a validated correlated- k model for the longwave, Journal of Geophysical Research: Atmospheres, 102(D14), 16663-16682, https://doi.org/10.1029/97JD00237, 1997.

Nakanishi, M., & Niino, H.: An improved Mellor–Yamada level-3 model: Its numerical stability and application to a regional prediction of advection fog, Boundary-Layer Meteorology, 119(2), 397-407, https://doi.org/10.1007/s10546-005-9030-8, 2006.

Nakanishi, M., & Niino, H.: Development of an improved turbulence closure model for the atmospheric boundary layer, Journal of the Meteorological Society of Japan. Ser. II, 87(5), 895-912, https://doi.org/10.2151/jmsj.87.895, 2009.

O'Brien, T. A., Li, F., Collins, W. D., Rauscher, S. A., Ringler, T. D., Taylor, M., ... & Leung, L. R.: Observed scaling in clouds and precipitation and scale incognizance in regional to global atmospheric models, Journal of Climate, 26(23), 9313-9333, https://doi.org/10.1175/JCLI-D-13-00005.1, 2013.

Park, S. H., Skamarock, W. C., Klemp, J. B., Fowler, L. D., & Duda, M. G.: Evaluation of global atmospheric solvers using extensions of the Jablonowski and Williamson baroclinic wave test case, Monthly Weather Review, 141(9), 3116-3129, https://doi.org/10.1175/MWR-D-12-00096.1, 2013.

Pedersen, C. A., & Winther, J. G.: Intercomparison and validation of snow albedo parameterization schemes in climate models, Climate Dynamics, 25(4), 351-362, https://doi.org/10.1007/s00382-005-0037-0, 2005.

Prein, A. F., Langhans, W., Fosser, G., Ferrone, A., Ban, N., Goergen, K., ... & Brisson, E.: A review on regional convection- permitting climate modeling: Demonstrations, prospects, and challenges, Reviews of geophysics, 53(2), 323-361, https://doi.org/10.1002/2014RG000475, 2015.

Geosci. Model Dev. Discuss., https://doi.org/10.5194/gmd-2018-340
Manuscript under review for journal Geosci. Model Dev.
Discussion started: 12 February 2019

Geoscientific Model Development Discussions
Open Access

Prein, A. F., Rasmussen, R. M., Ikeda, K., Liu, C., Clark, M. P., & Holland, G. J.: The future intensification of hourly precipitation extremes, Nature Climate Change, 7(1), 48, https://doi.org/10.1038/nclimate3168, 2017.

Rauscher, S. A., Ringler, T. D., Skamarock, W. C., & Mirin, A. A.: Exploring a global multiresolution modeling approach using aquaplanet simulations, Journal of Climate, 26(8), 2432-2452, https://doi.org/10.1175/JCLI-D-12-00154.1, 2013.

Ringler, T. D., Jacobsen, D., Gunzburger, M., Ju, L., Duda, M., & Skamarock, W.: Exploring a multiresolution modeling approach within the shallow-water equations, Monthly Weather Review, 139(11), 3348-3368, https://doi.org/10.1175/MWR-D-10-05049.1, 2011.

Ringler, T., Ju, L., & Gunzburger, M.: A multiresolution method for climate system modeling: Application of spherical centroidal Voronoi tessellations, Ocean Dynamics, 58(5-6), 475-498, https://doi.org/10.1007/s10236-008-0157-2, 2008.

Sakaguchi, K., Leung, L. R., Zhao, C., Yang, Q., Lu, J., Hagos, S., ... & Lauritzen, P. H.: Exploring a multiresolution approach using AMIP simulations, Journal of Climate, 28(14), 5549-5574, https://doi.org/10.1175/JCLI-D-14-00729.1, 2015.

Sakaguchi, K., Lu, J., Leung, L. R., Zhao, C., Li, Y., & Hagos, S.: Sources and pathways of the upscale effects on the Southern Hemisphere jet in MPAS- CAM4 variable-resolution simulations, Journal of Advances in Modeling Earth Systems, 8(4), 1786-1805, https://doi.org/10.1002/2016MS000743, 2016.Skamarock, W. C., & Gassmann, A.: Conservative transport schemes for spherical geodesic grids: High-order flux operators for ODE-based time integration, Monthly Weather Review, 139(9), 2962-2975, https://doi.org/10.1175/MWR-D-10-05056.1, 2011.

Skamarock, W. C., & Klemp, J. B.: A time-split nonhydrostatic atmospheric model for weather research and forecasting applications, Journal of Computational Physics, 227(7), 3465-3485, https://doi.org/10.1016/j.jcp.2007.01.037, 2008.

Skamarock, W. C., Klemp, J. B., Duda, M. G., Fowler, L. D., Park, S. H., & Ringler, T. D.: A multiscale nonhydrostatic atmospheric model using centroidal Voronoi tesselations and C-grid staggering, Monthly Weather Review, 140(9), 3090-3105, https://doi.org/10.1175/MWR-D-11-00215.1, 2012.

Sukovich, E. M., Ralph, F. M., Barthold, F. E., Reynolds, D. W., & Novak, D. R.: Extreme quantitative precipitation forecast performance at the Weather Prediction Center from 2001 to 2011, Weather and Forecasting, 29(4), 894-911, https://doi.org/10.1175/WAF-D-13-00061.1, 2014.

Geosci. Model Dev. Discuss., https://doi.org/10.5194/gmd-2018-340
Manuscript under review for journal Geosci. Model Dev.
Discussion started: 12 February 2019

Thompson, G., Field, P. R., Rasmussen, R. M., & Hall, W. D.: Explicit forecasts of winter precipitation using an improved bulk microphysics scheme. Part II: Implementation of a new snow parameterization, Monthly Weather Review, 136(12), 5095-5115, https://doi.org/10.1175/2008MWR2387.1, 2008.

Wang, Y., Leung, L. R., McGREGOR, J. L., Lee, D. K., Wang, W. C., Ding, Y., & Kimura, F.: Regional climate modeling: progress, challenges, and prospects, Journal of the Meteorological Society of Japan. Ser. II, 82(6), 1599-1628, https://doi.org/10.2151/jmsj.82.1599, 2004.

Wicker, L. J., & Skamarock, W. C.: Time-splitting methods for elastic models using forward time schemes, Monthly weather review, 130(8), 2088-2097, https://doi.org/10.1175/1520-0493(2002)130<2088:TSMFEM>2.0.CO;2, 2002.

Xu, H., & Yao, W.: A numerical study of the Beijing extreme rainfall of 21 July 2012 and the impact of topography, Advances in Meteorology, http://dx.doi.org/10.1155/2015/980747, 2015.

Yang, Q., Leung, L. R., Rauscher, S. A., Ringler, T. D., & Taylor, M. A.: Atmospheric moisture budget and spatial resolution dependence of precipitation extremes in aquaplanet simulations, Journal of Climate, 27(10), 3565-3581, https://doi.org/10.1175/JCLI-D-13-00468.1, 2014.

Yang, Q., R. Houze, Jr., L.R. Leung, & Z. Feng : Environments of long-lived mesoscale convective systems over the Central United States in convection permitting climate simulations, J. Geophys. Res., 122, https://doi.org/ 10.1002/2017JD027033, 2017.

Yessad, K., & Bénard, P.: Introduction of a local mapping factor in the spectral part of the Météo-France global variable mesh numerical forecast model, Quarterly Journal of the Royal Meteorological Society, 122(535), 1701-1719, https://doi.org/10.1002/qj.49712253511, 1996.

Zarzycki, C. M., Levy, M. N., Jablonowski, C., Overfelt, J. R., Taylor, M. A., & Ullrich, P. A.: Aquaplanet experiments using CAM's variable-resolution dynamical core, Journal of Climate, 27(14), 5481-5503, https://doi.org/10.1175/JCLI-D-14-00004.1, 2014.

Zhang, D. L., Lin, Y., Zhao, P., Yu, X., Wang, S., Kang, H., & Ding, Y.: The Beijing extreme rainfall of 21 July 2012:"Right results" but for wrong reasons, Geophysical Research Letters, 40(7), 1426-1431, https://doi.org/10.1002/grl.50304, 2013.

Zhang, H., & Zhai, P.: Temporal and spatial characteristics of extreme hourly precipitation over eastern China in the warm season, Advances in atmospheric sciences, 28(5), 1177, https://doi.org/10.1007/s00376-011-0020-0, 2011.

Zhang, L., Dong, M., & Wu, T.: Changes in precipitation extremes over eastern China simulated by the Beijing Climate Center Climate System Model (BCC_CSM1. 0), Climate Research, 50(2-3), 227-245, https://doi.org/10.3354/cr01066, 2011.

Zhang, Q., Xiao, M., Singh, V. P., Liu, L., & Xu, C. Y.: Observational evidence of summer precipitation deficit-temperature coupling in China, Journal of Geophysical Research: Atmospheres, 120(19), https://doi.org/10.1002/2015JD023830, 2015.

Zhang, Q., Zheng, Y., Singh, V. P., Luo, M., & Xie, Z.: Summer extreme precipitation in eastern China: Mechanisms and impacts, Journal of Geophysical Research: Atmospheres, 122(5), 2766-2778, https://doi.org/10.1002/2016JD025913, 2017.

Zhang,Y., P., L., & Zhong, Q.: An interdecadal change in the relationship between the western North Pacific Ocean and the East Asian summer monsoon, Climate Dynamics, 49(4), 1139-1156, https://doi.org/10.1007/s00382-016-3370-6, 2017.

Zhai, P., Zhang, X., Wan, H., & Pan, X.: Trends in total precipitation and frequency of daily precipitation extremes over China, Journal of Climate, 18(7), 1096-1108, https://doi.org/10.1175/JCLI-3318.1, 2005.

Zhao, C., Leung, L. R., Park, S. H., Hagos, S., Lu, J., Sakaguchi, K., ... & Duda, M. G.: Exploring the impacts of physics and resolution on aqua,planet simulations from a nonhydrostatic global variablemresolution modeling framework, Journal of Advances in Modeling Earth Systems, 8(4), 1751-1768, https://doi.org/10.1002/2016MS000727, 2016.

Zhao, Y., Xu, X., Zhao, T., Xu, H., Mao, F., Sun, H., & Wang, Y.: Extreme precipitation events in East China and associated moisture transport pathways, Science China Earth Sciences, 59(9), 1854-1872, https://doi.org/10.1007/s11430-016-5315-7, 2016.

Zheng, Y., Xue, M., Li, B., Chen, J., & Tao, Z.: Spatial characteristics of extreme rainfall over China with hourly through 24-hour accumulation periods based on national-level hourly rain gauge data, Advances in Atmospheric Sciences, 33(11), 1218-1232, https://doi.org/10.1007/s00376-016-6128-5, 2016.

Zhong, S., pQian, Y., Zhao, C., Leung, R., & Yang, X. Q.: A case study of urbanization impact on summer preciitation in the Greater Beijing Metropolitan Area: Urban heat island versus aerosol effects, Journal of Geophysical Research: Atmospheres, 120(20), 10-903, https://doi.org/10.1002/2015JD023753, 2015.

Zhong, S., Qian, Y., Zhao, C., Leung, R., Wang, H., Yang, B., ... & Liu, D.: Urbanization-induced urban heat island and aerosol effects on climate extremes in the Yangtze River Delta region of China, Atmospheric Chemistry and Physics, 17(8), 5439-5457, https://doi.org/10.5194/acp-17-5439-2017, 2017.

Zhou, T. J., & Li, Z.: Simulation of the East Asian summer monsoon using a variable resolution atmospheric GCM, Climate Dynamics, 19(2), 167-180, https://doi.org/10.1007/s00382-001-0214-8, 2002.

Geosci. Model Dev. Discuss., https://doi.org/10.5194/gmd-2018-340
Manuscript under review for journal Geosci. Model Dev.
Discussion started: 12 February 2019

Geoscientific Model Development Discussions
Open Access
EGU

Table 1 Numerical Experiments conducted and analyzed in this study

Physics/Resolution	MPAS				
	U15km	U60km	V30km	V16km	V4km
WSM6+NTD	Yes	/	/	Yes	/
WSM6+GF	Yes	Yes	Yes	Yes	Yes
Thompson+GF	/	/	/	/	Yes

Geosci. Model Dev. Discuss., https://doi.org/10.5194/gmd-2018-340
Manuscript under review for journal Geosci. Model Dev.
Discussion started: 12 February 2019

Geoscientific Model Development Discussions

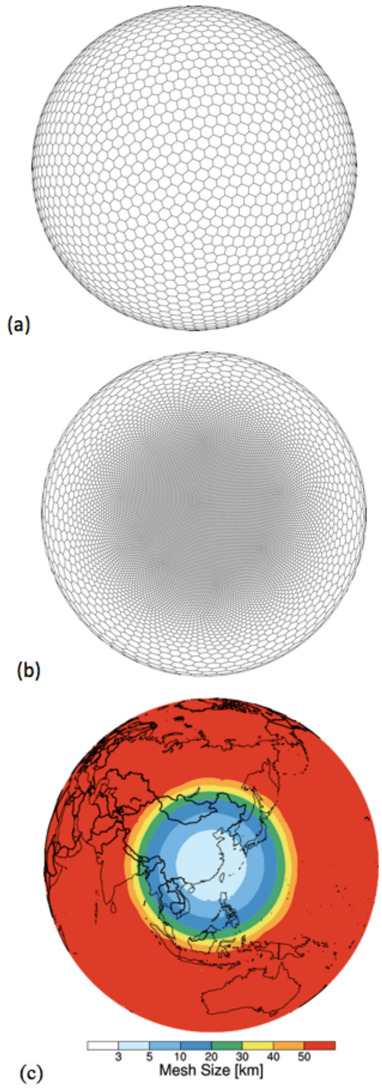

Figure 1 (a) quasi-uniform mesh and (b) variable-resolution mesh used in the MPAS experiments. Both meshes are plotted at resolutions significantly lower than used in the experiments to show the mesh cells. (c) global variable-resolution mesh size distribution in the variable resolution 4-60 km experiment.

Geosci. Model Dev. Discuss., https://doi.org/10.5194/gmd-2018-340
Manuscript under review for journal Geosci. Model Dev.
Discussion started: 12 February 2019

Geoscientific Model Development
Discussions
Open Access

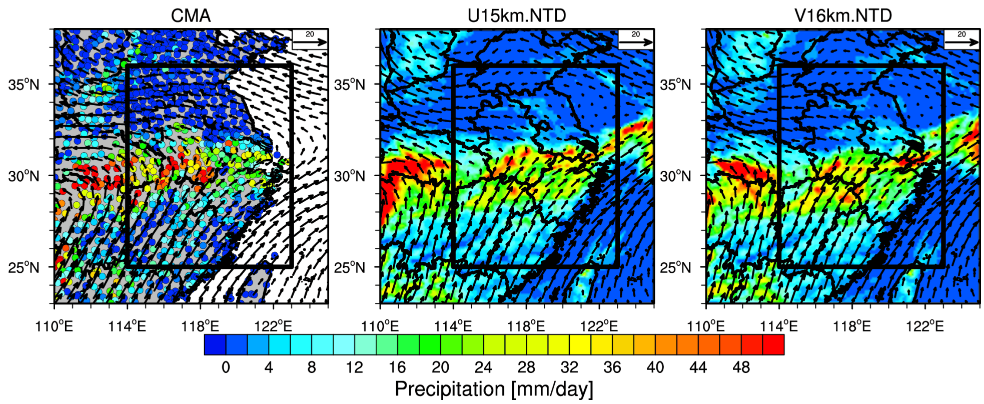

Figure 2 Spatial distributions of precipitation and wind fields at 850 hPa averaged during the event (June 25 00:00 to June 27 12:00 UTC time) from the simulations with the global uniform (15 km) and variable (16 km over the refined region as shown in Fig. 1c) resolutions. The observed mean precipitation from the CMA stations and the wind fields from the ERA-interim reanalysis are shown. The black box denotes the region for the analysis in the following.

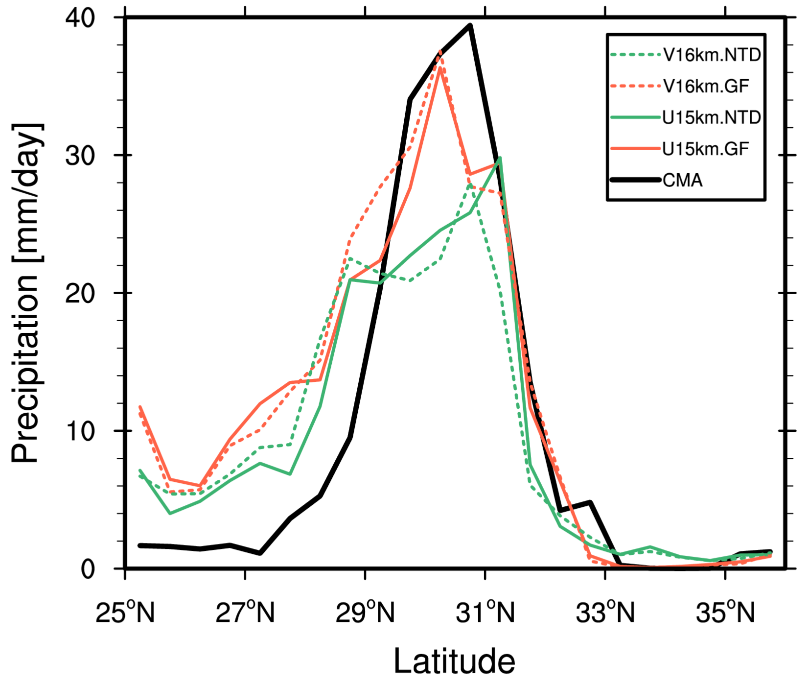

Figure 3 Zonal distributions of precipitation averaged during the event (June 25 00:00 to June 27 12:00 UTC time) over East China (denoted as the black box in Fig. 2) from the CMA station observations and the simulations with the global uniform (15 km, solid lines) and variable (16 km over the refined region as shown in Fig. 1c, dash lines) resolutions with two convective parameterizations (GF, red lines; NTD, green lines). The modeling results are sampled at the CMA station.

Geosci. Model Dev. Discuss., https://doi.org/10.5194/gmd-2018-340
Manuscript under review for journal Geosci. Model Dev.
Discussion started: 12 February 2019

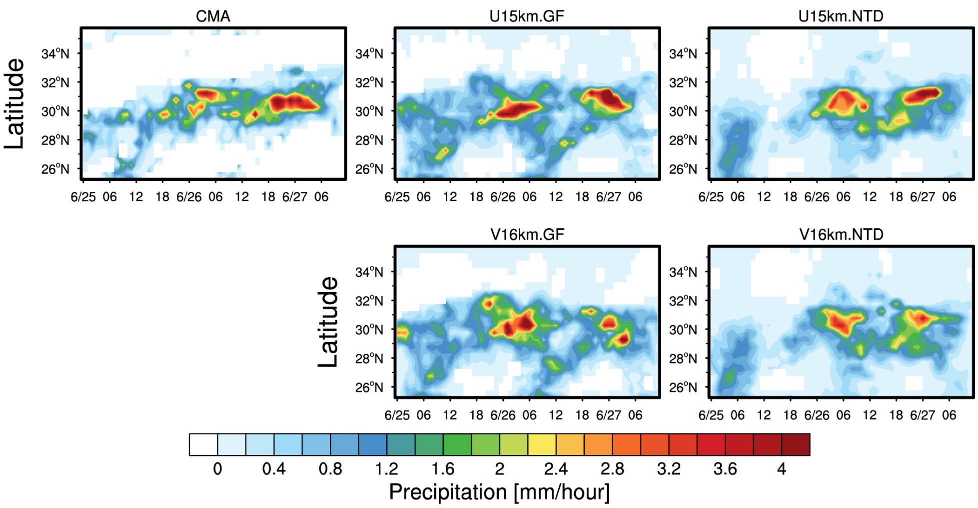

Figure 4 Time-Latitude cross section of precipitation during the event over East China from the CMA station observations and the simulations with the global uniform and variable resolutions with two convective parameterizations. The modeling results are sampled at the CMA stations.

Geosci. Model Dev. Discuss., https://doi.org/10.5194/gmd-2018-340
Manuscript under review for journal Geosci. Model Dev.
Discussion started: 12 February 2019

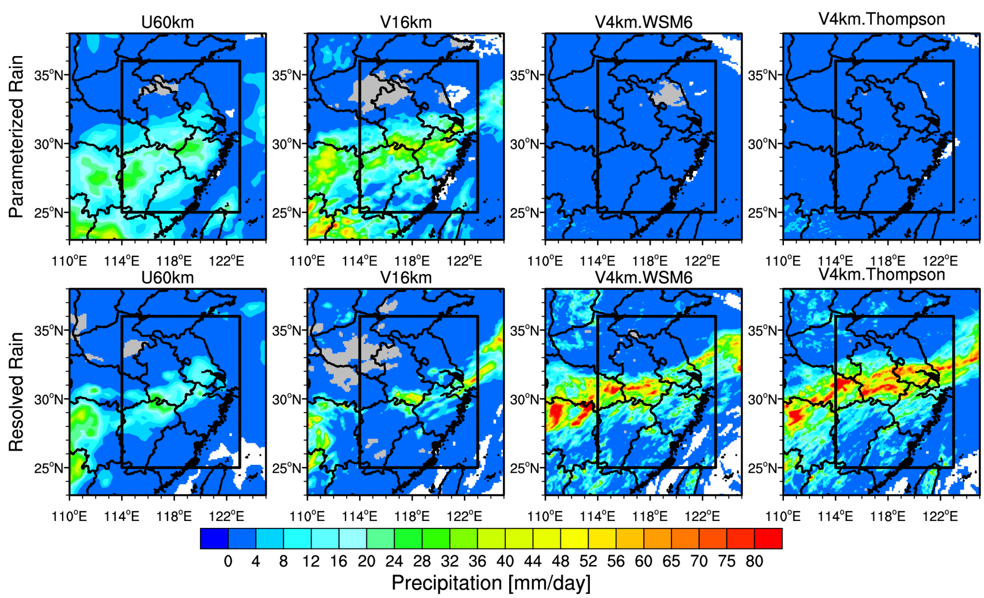

Figure 5 Spatial distribution of averaged parameterized and resolved precipitation during the event over East China from the simulations with the resolutions of 60 km, 16 km, and 4 km.

Geosci. Model Dev. Discuss., https://doi.org/10.5194/gmd-2018-340
Manuscript under review for journal Geosci. Model Dev.
Discussion started: 12 February 2019

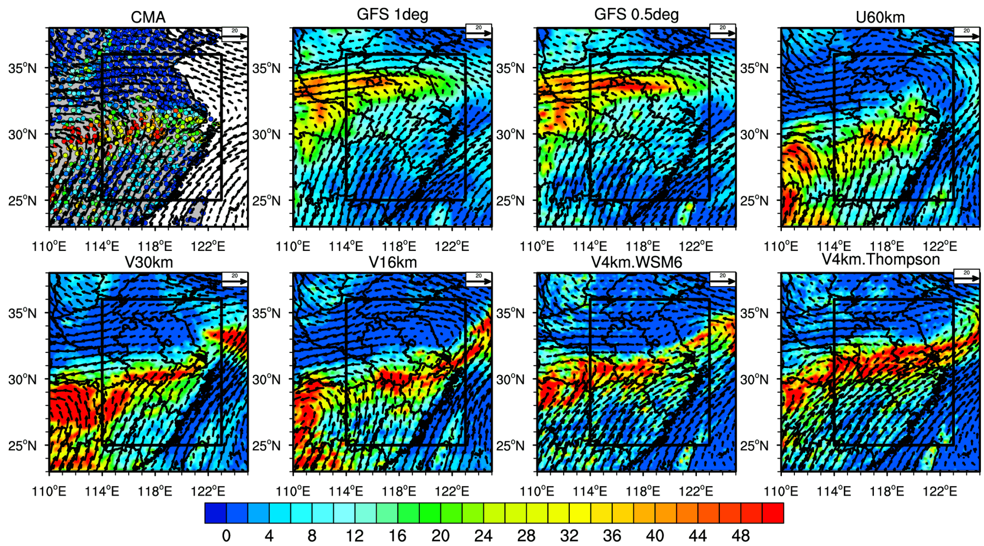

Figure 6 Spatial distributions of precipitation and wind fields at 850 hPa averaged during the event from the MPAS simulations at the resolutions of 60 km, 30 km, 16 km, and 4 km. The observed mean precipitation from the CMA stations and the wind fields from the ERA-interim reanalysis are shown as well. The black box denotes the region for the analysis in the following. For comparison, the GFS forecasts at 1 degree and 0.5 degree resolutions are also shown.

Geosci. Model Dev. Discuss., https://doi.org/10.5194/gmd-2018-340
Manuscript under review for journal Geosci. Model Dev.
Discussion started: 12 February 2019

Geoscientific Model Development Discussions
Open Access

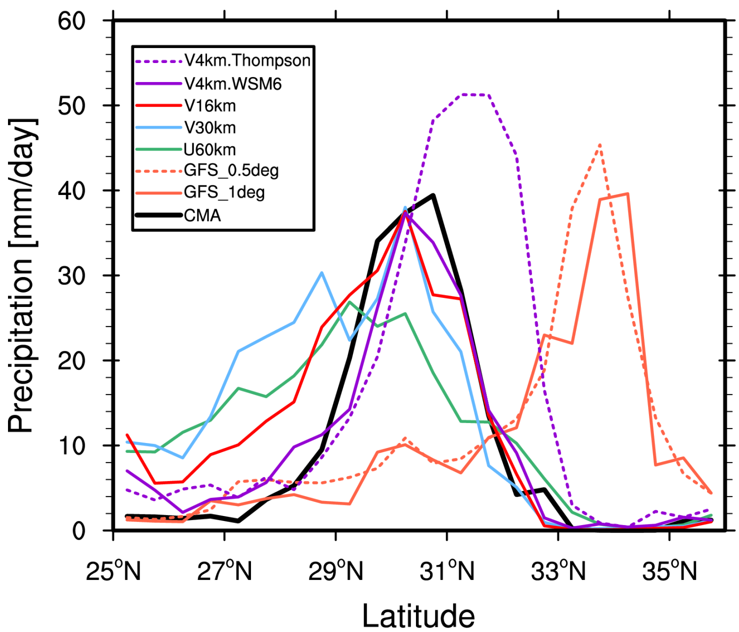

Figure 7 Zonal distributions of precipitation averaged during the event over East China from the CMA station observations and the simulations with the resolutions of 60 km, 30 km, 16 km, and 4 km. For comparison, the GFS forecasts at 1 degree and 0.5 degree resolutions are also included. The modeling results are sampled at the CMA stations.

Geosci. Model Dev. Discuss., https://doi.org/10.5194/gmd-2018-340
Manuscript under review for journal Geosci. Model Dev.
Discussion started: 12 February 2019

Geoscientific Model Development Discussions
Open Access

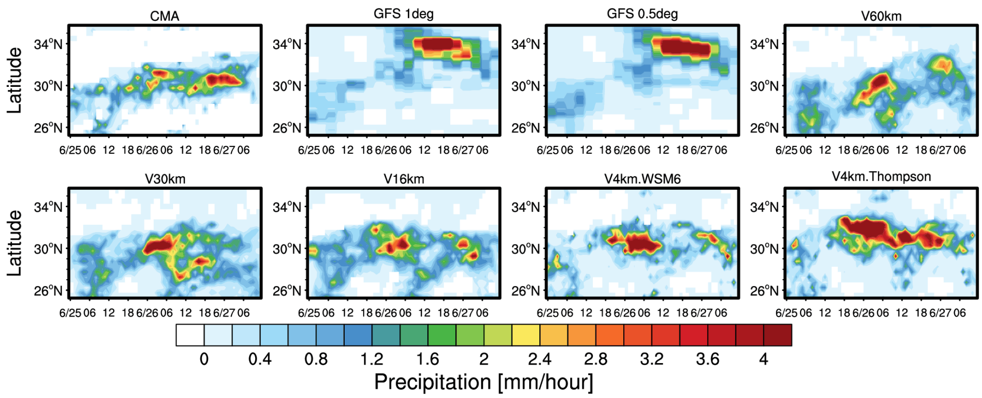

Figure 8 Time-Latitude cross section of precipitation during the event over East China from the CMA station observations, GFS forecasts at 0.5° and 1.0° resolutions, and the MPAS simulations at resolutions of 60 km, 30 km, 16 km, and 4 km over East China. The simulations at 4 km are with two cloud microphysics schemes (WSM6 and Thompson). The modeling results are sampled at the CMA stations.

Geosci. Model Dev. Discuss., https://doi.org/10.5194/gmd-2018-340
Manuscript under review for journal Geosci. Model Dev.
Discussion started: 12 February 2019

Geoscientific Model Development Discussions
Open Access

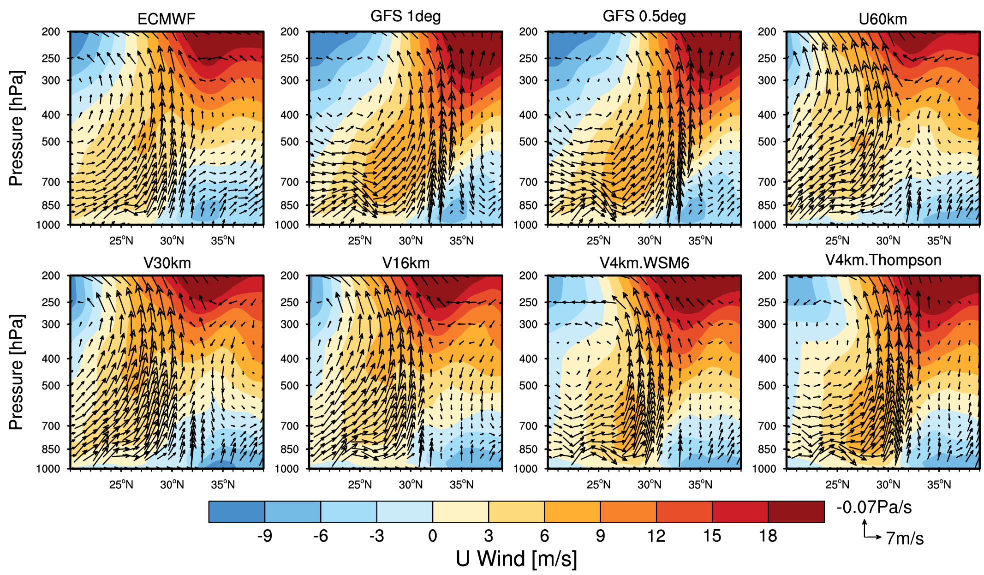

Figure 9 Height-Latitude cross section of wind fields averaged over the region (as shown in Fig. 6) during the event from the ERA-interim reanalysis, the GFS forecasts at 0.5° and 1.0° resolutions, and the MPAS simulations at resolutions of 60 km, 30 km, 16 km, and 4 km. The simulations at 4 km are with two cloud microphysics schemes (WSM6 and Thompson). The positive color represents eastward wind.

Geosci. Model Dev. Discuss., https://doi.org/10.5194/gmd-2018-340
Manuscript under review for journal Geosci. Model Dev.
Discussion started: 12 February 2019

Geoscientific Model Development Discussions
Open Access
EGU

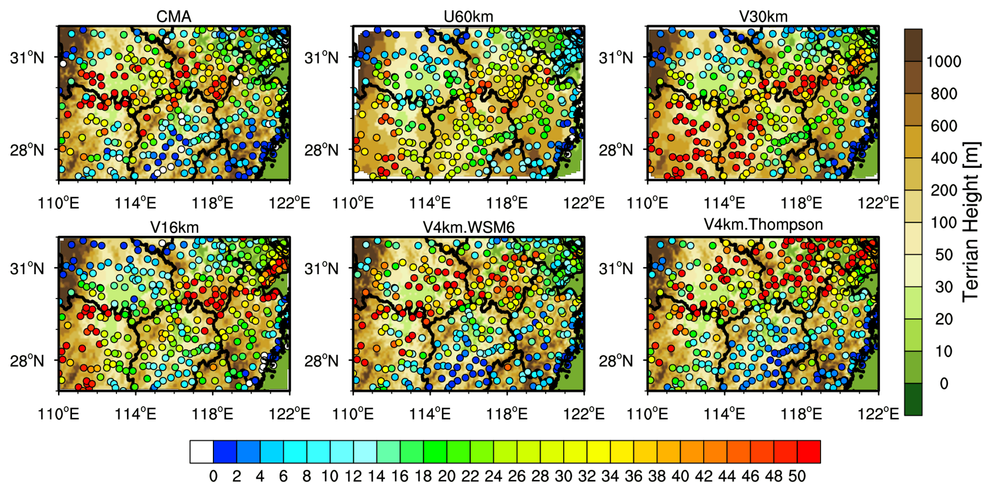

Figure 10 Spatial distributions of precipitation averaged during the event over the heavy precipitation region (27°N-32°N and 110°E-122°E) from the CMA observations and the MPAS simulations at the resolutions of 60 km, 30 km, 16 km, and 4 km. The simulations are sampled at the CMA stations. The topography is also shown.

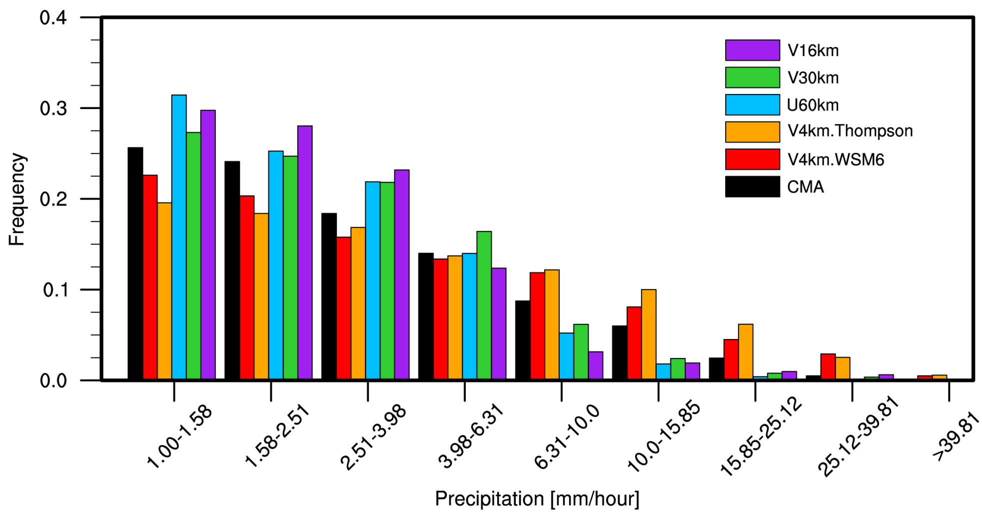

Figure 11 Probability density functions (PDFs) of hourly precipitation at all the CMA stations during the event over East China from the CMA observations and the MPAS simulations at the resolutions of 60 km, 30 km, 16 km, and 4 km. The simulations are sampled at the CMA stations.

Geosci. Model Dev. Discuss., https://doi.org/10.5194/gmd-2018-340
Manuscript under review for journal Geosci. Model Dev.
Discussion started: 12 February 2019

Geoscientific Model Development Discussions
Open Access

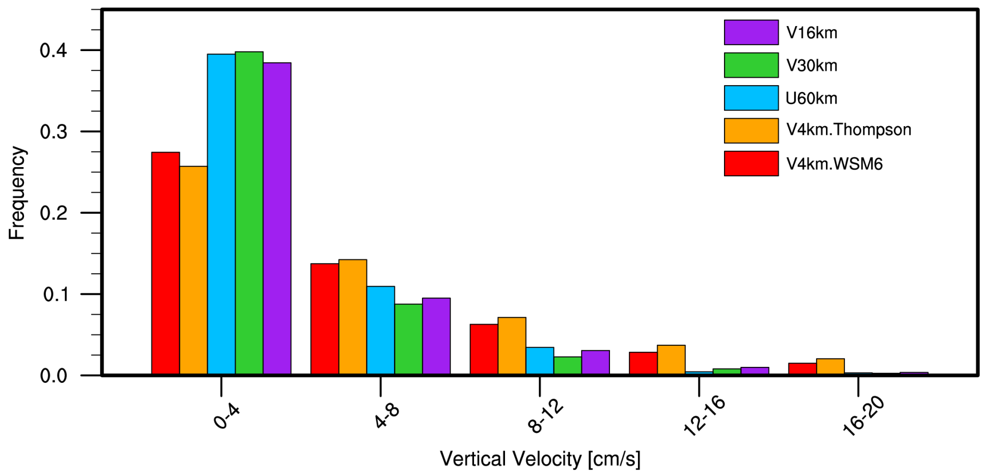

Figure 12 Probability density functions (PDFs) of hourly upward vertical velocity averaged below 700 hPa at all the CMA stations during the event over East China from the MPAS simulations at the resolutions of 60 km, 30 km, 16 km, and 4 km.